11th World Congress on Computational Mechanics (WCCM XI)
5th European Conference on Computational Mechanics (ECCM V)
6th European Conference on Computational Fluid Dynamics (ECFD VI)
E. Oñate, J. Oliver and A. Huerta (Eds)

FURTHER VALIDATIONS OF PENALIZATION AND VIC BASED METHODS FOR AERONAUTIC APPLICATIONS

F MORENCY* AND H. BEAUGENDRE†

* Professor, TFT Laboratory, Mechanical Engineering Department
École de technologie supérieure
Montréal, Canada.
e-mail: francois.morency@etsmtl.ca, web page: http://www.cimne.com/

†IMB, UMR 5251 et Inria Bordeaux Sud-Ouest
Université de Bordeaux
F-33400 Talence, France
e-mail: heloise.beaugendre@math.u-bordeaux1.fr

Key words: Oscillating-airfoil, Vortex in Cell, Penalization, Aerodynamic forces

Abstract. The fluid-solid interaction method proposed in this work is formulated for a laminar flow modeled by the incompressible Navier-Stokes equations in which we consider the presence of a rigid moving solid S^i. The model is formulated inside an immersed boundary method based on a penalization technique to account for rigid body. The penalization technique extend the velocity field inside the solid body and use a penalty term to enforce the rigid motion inside the solid. The method is used to study the case of an oscillating airfoil in large flapping motion. A method appropriate for the calculation of forces and angular momentum with penalized equations method is proposed and validated. The effect of geometries on the aerodynamic forces and the angular momentum is investigated, especially the airfoil thickness. For propulsion and power extraction, the results are similar to the one available in literature. As the airfoil thickness increase the maximum values decrease slightly, but the airfoil shape as only a small effects on results.

1 INTRODUCTION

Computations by classical computational fluid dynamics (CFD) codes use body fitted grid to discretize the computational domain. On the other hand, flow simulations by the immersed boundary methods (IBM) use a grid that does not follow the body geometry of the body. Most of the difficulties associated with grid generation are avoided. IBM can easily model flows around complex geometries in large motion[1]. The Cartesian grids used with the IBM limits the application to Euler or Laminar flow, unless local grid refinement strategy[2] and specific turbulent wall model are used[3]. IBMs are seldom

used to solve aeronautical flows, although methodological advances allow simulation of compressible flows at high Reynolds numbers[4]. The penalization method used in this work is a special case of the IBM, where bodies are considered as porous media with a very small permeability[5]. The penalization method has the advantage of avoiding the tasks of tracking the fluid solid interfaces into the grid and the related interpolation of the forcing term.

Because IBMs can easily handle large motion, they are used to simulate flow around small size unmanned aerial vehicule that operate in low Reynolds number regime. At low Reynolds number, fixed wing geometry performances decrease. A solution that worth investigation is the use of unconventional concept such as flapping wings to build small aircraft that can fly efficiently[6, 7]. Flapping motion can also be used to extract energy from wind or river[8]. There is several parameters that determine the propulsion efficiency in flapping motion: the heaving amplitude, the pitching amplitude, the frequency and the geometry. With IBMs, the study of the geometry effects on the propulsion or power extraction is relatively easy. Until better shapes are devised, classical NACA airfoil geometries are a good starting point to explore the design space.

In this paper, we propose to extend the use of an IBM [9] that combines the advantage of the penalization and of the Vortex-in-Cell (VIC) methods, namely no restriction on CFL number, for simulations of airfoils in flapping motion. The first specific objective is to validate the force and momentum calculations within the IBM. Force calculations at interface is always a challenge in IBM because the mesh does not follow the fluid solid interface. A second specific objective is to study the geometry effects, and especially geometry thickness, on the power extraction and propulsion regime. First, the penalized Navier-Stokes equations are presented. Then the numerical method based on VIC scheme is explained together with the strategy used to compute the force and moment exerted by fluid on airfoil. Finally, the oscillating airfoil test case is presented, results are validated against literature and geometry effects are studied.

2 Penalization

The fluid-solid interaction flow model proposed in this work is based on an incompressible laminar Newtonian flow around a body considered as rigid (without any deformation) and delimited by level-set functions. The mass and momentum conservation equations are

$$\nabla \cdot \mathbf{u} = 0 \quad \text{in } \Omega \tag{1a}$$

$$\frac{\partial \mathbf{u}}{\partial t} + (\mathbf{u} \cdot \nabla)\,\mathbf{u} - \nu \nabla^2 \mathbf{u} + \frac{1}{\rho}\nabla p = 0 \quad \text{in } \Omega. \tag{1b}$$

where $\mathbf{u}$ is the velocity vector, $\nu = \mu/\rho$ is the kinematic viscosity, ρ is the density, and p is the pressure. Now we consider, in Ω, the presence of a rigid moving solid S^i. The boundary of S^i is computed from a level set function Φ_{s^i}. Φ_{s^i} is the signed distance

function to S^i, typically Φ_{s^i} will be negative inside the object and positive outside. The penalization extend the velocity field inside the solid body and solve the flow equations with a penalization term to enforce rigid motion inside the solid as proposed by [10].

Let $\mathbf{u}_{s^i}$ be the rigid moving body velocity vector of S^i. Inside S^i, the momentum equation becomes $\mathbf{u} = \mathbf{u}_{s^i}$ and remains equation (1b) outside S^i. This is summarized as follows: given a very large penalization parameter, $\lambda \gg 1$ and denoting by χ_{s^i} the characteristic function of the solid S^i is $\chi_{s^i} = 1$ inside S^i and $\chi_{s^i} = 0$ outside S^i.

The model equation is given by

$$\frac{\partial \mathbf{u}}{\partial t} + (\mathbf{u} \cdot \nabla)\,\mathbf{u} - \nu \nabla^2 \mathbf{u} + \frac{1}{\rho}\nabla p = \lambda \chi_{s^i}(\mathbf{u}_{s^i} - \mathbf{u}) \qquad \text{for } \mathbf{x} \in \Omega \text{ and } t > 0, \tag{2}$$

coupled with the incompressible mass conservation (1a). This model can easily be generalized to multiple rigid bodies S^i.

To solve our governing equations the following strategies have been chosen:

1. A vortex formulation of our governing equations is used: this formulation is especially adapted to study oscillatory motion that create large flow separation around aerodynamic bodies.

2. A vortex in cell (VIC) scheme is used to solve the equation: this scheme offers less CFL restrictions.

3. A time splitting algorithm allows to take into account the specific requirement of each equation term, for example the implicit treatment of the penalization term for accuracy purpose.

Let us consider the penalized Navier-Stokes equation in the vorticity formulation by applying the **curl** operator to equation (2), with $\boldsymbol{\omega} = \nabla \times \mathbf{u}$ in Ω

$$\begin{aligned} \frac{\partial \boldsymbol{\omega}}{\partial t} + (\mathbf{u} \cdot \nabla)\,\boldsymbol{\omega} &= (\boldsymbol{\omega} \cdot \nabla)\,\mathbf{u} + \nu \nabla^2 \boldsymbol{\omega} + \lambda \nabla \times [H(\Phi_{s^i})(\mathbf{u}_{s^i} - \mathbf{u})] && (3) \\ \nabla \cdot \mathbf{u} &= 0 && (4) \end{aligned}$$

3 VIC SCHEME

The Vortex-In-Cell (VIC) scheme computes the non linear advection by tracking the trajectories of the Lagrangian particles through a set of ODEs. An Eulerian grid is adopted to solve the velocity field, the diffusive term, and the penalization term. Given $D/Dt(\cdot)$, the material derivative, and expanding the penalization term, equation (2) becomes

$$\frac{D\boldsymbol{\omega}}{Dt} = (\boldsymbol{\omega} \cdot \nabla)\,\mathbf{u} + \nu \nabla^2 \boldsymbol{\omega} + \lambda H(\Phi_{s^i})\,(\boldsymbol{\omega}_{s^i} - \boldsymbol{\omega}) + \lambda \delta(\Phi_{s^i})\,[\nabla(\Phi_{s^i}) \times (\mathbf{u}_{s^i} - \mathbf{u})]\,, \tag{5}$$

where $\delta(\Phi_{s^i})$ is the 1D Dirac delta function and $\boldsymbol{\omega}_{s^i} = \nabla \times \mathbf{u}_{s^i}$.

The domain Ω is meshed using a uniform fixed cartesian grid. We denote the time step Δt, such that $t^n = n\Delta t$ and $\Phi^n_{s^i}$, $\mathbf{u}^n$, $\boldsymbol{\omega}^n$ are grid values of the level set functions, velocity, and vorticity. The vorticity field $\boldsymbol{\omega}$ is represented by a set of particles

$$\boldsymbol{\omega}(\mathbf{x}) = \sum_{p=1}^{N} v_p \boldsymbol{\omega}_p \zeta\left(\mathbf{x} - \mathbf{x}_p\right), \tag{6}$$

where N is the number of particles, $\mathbf{x}_p$ the particle location, v_p and $\boldsymbol{\omega}_p$ are the volume and the strength of a general particle p. ζ is a smooth distribution function, such that $\int \zeta(x)\, dx = 1$, which acts on the vortex support.

A viscous splitting algorithm solve the equation (3). Each time step Δt is solved using three sub-steps as follows.

$$1 - \text{Advection:} \quad \frac{D\boldsymbol{\omega}}{Dt} = \frac{\partial \boldsymbol{\omega}}{\partial t} + \left(\mathbf{u} \cdot \nabla\right)\boldsymbol{\omega} = 0. \tag{7a}$$

$$2 - \text{Stretching and diffusion:} \quad \frac{\partial \boldsymbol{\omega}}{\partial t} = \left(\boldsymbol{\omega} \cdot \nabla\right)\mathbf{u} + \nu \nabla^2 \boldsymbol{\omega}. \tag{7b}$$

$$3 - \text{Penalization term:} \quad \frac{\partial \boldsymbol{\omega}}{\partial t} = \lambda \nabla \times \left(H\left(\Phi_{s^i}\right)\left(\mathbf{u}_{s^i} - \mathbf{u}\right)\right). \tag{7c}$$

sub-step 1: advection
Grid vorticity above a certain cut-off value will create particles at grid point locations [11]. Then, using equation (7a), particles are displaced with a fourth order Runge-Kutta time-stepping scheme. From the new vortex particles' location, the vorticity field is remeshed on the grid by the M'_4 third order interpolation kernel introduced by [12].

sub-step 2 : stretching and diffusion
The equation to solve for vortex stretching and viscous contribution is given by equation (7b) which is approximated onto the grid with an Euler explicit scheme, while the Laplacian is evaluated, with a second order accurate standard five points stencil.

sub-step 3: penalization
The penalization term is evaluated using equation (7c). In our simulations, λ is fixed to $10^8/\Delta t$. An implicit Euler time discretization is used for the penalization term in the Navier-Stokes equation:

$$\mathbf{u}^{n+1} = \frac{\mathbf{u}^\star + \lambda \Delta t H(\Phi_{s^i}) \mathbf{u}^n_{s^i}}{1 + \Delta t H(\Phi_{s^i})}. \tag{8}$$

where $\mathbf{u}^\star$ is the velocity after sub-step 2. The vorticity field at t^{n+1} is evaluated on the grid by taking the **curl** of the velocity, $\boldsymbol{\omega}^{n+1} = \nabla \times \mathbf{u}^{n+1}$, and computing the derivative through the second order centred finite differences approximation. This method is unconditionally stable.

Since the incompressible velocity field is divergence-free, from the vector field theory, we can define a vector potential $\boldsymbol{\psi}$ such that $\mathbf{u} = \nabla \times \boldsymbol{\psi}$. The vector potential $\boldsymbol{\psi}$ is a

3D extension of the stream function ψ. This potential vector is imposed to be solenoidal $\nabla \cdot \boldsymbol{\psi} = 0$ and given $\boldsymbol{\omega}^{n+1}$ the updated vorticity field, the stream function field is computed by solving the linear Poisson equation $\nabla^2 \boldsymbol{\psi} = -\boldsymbol{\omega}$ on the cartesian grid with boundary conditions on $\partial\Omega$. In equation (8), $\mathbf{u}^\star$ is computed with $\boldsymbol{\omega}^\star$ the vorticity resulting from sub-step 2.

3.1 Aerodynamic forces on solid

The penalization term in equation (3), the last term on the right hand side, can also be considered as being the rigid body effect on fluid. At each time step, the penalization term forces the velocity inside the rigid body S^i to be equal to $\mathbf{u}_{s^i}$. The momentum change caused by the penalization is computed by

$$\Delta \mathbf{m} = \int_{S^i} \rho(\mathbf{u} - \mathbf{u}_{s^i}) d\mathbf{x}. \tag{9}$$

This change of momentum happens during one time step Δt. Thus the force is $\mathbf{F} = \frac{\Delta \mathbf{m}}{\Delta t}$.

In a similar way, the angular momentum change created by the penalization term is

$$\Delta \mathbf{m}_\theta = \int_{S^i} \rho \mathbf{r} \times (\mathbf{u} - \mathbf{u}_{s^i}) d\mathbf{x}. \tag{10}$$

The instantaneous pitching moment is $\mathbf{T} = \frac{\Delta \mathbf{m}_\theta}{\Delta t}$.

In 2D flows, the drag, lift and pitching moment coefficients are defined respectively as

$$C_x = \frac{F_x}{1/2 \rho u_{ref}^2 c}; \quad C_y = \frac{F_y}{1/2 \rho u_{ref}^2 c}; \quad C_m = \frac{T}{1/2 \rho u_{ref}^2 c^2}. \tag{11}$$

where the x axis is aligned with the far field velocity vector $\mathbf{u}_{ref}$, the y axis is perpendicular to the far field velocity vector and c is the airfoil cord.

4 OSCILLATING AIRFOIL

In this test case, we model an oscillating wing experiencing simultaneous pitching $\theta(t)$ and heaving $h(t)$ motions. The infinitely long wing is based on a NACA 0015 airfoil. The pitching axis is located along the airfoil chord at the position $(x_p, y_p) = (1/3, 0)$. First one of the motions described by Kinsey and Dumas [8] is use to validate our numerical method. The airfoil motion is defined by the heaving $h(t)$ and the pitching angle $\theta(t)$ defined as follows:

$$\begin{cases} \theta(t) = \theta_0 \sin(\omega t) \\ h(t) = H_0 \sin(\omega t + \Phi) \end{cases} \tag{12}$$

where H_0 is the heaving amplitude and θ_0 is the pitching amplitude. The angular frequency is defined by $\omega = 2\pi f$ and the phase difference Φ is set to 90^o. The heaving velocity is then given by:

$$V_y(t) = H_0\omega\cos(\omega t + \Phi) \tag{13}$$

Based on the imposed motion and on the upstream flow conditions, the airfoil experiences an effective angle of attack $\alpha(t)$ and an effective upstream velocity $V_{eff}(t)$ defined by

$$\begin{cases} \alpha(t) = \arctan(-Vy(t)/U_\infty) - \theta(t) \\ V_{eff}(t) = \sqrt{\left(U_\infty^2 + V_y^2(t)\right)} \end{cases} \tag{14}$$

Depending on θ_0, there is two operating regimes: a power-extraction regime and a propulsion regime.

4.1 Validations against a power extraction and a propulsion case

If we made visible the effective angle of attack $\alpha(t)$ from the apparent trajectory of the airfoil we can draw the force F acting on the airfoil. $F = L + D$ where L is the lift force and D is the drag force. If the vertical component L is in the same direction as the vertical displacement of the airfoil, the flow makes a positive work on the airfoil : this is a power extraction regime else we face a propulsion regime.

A power-extraction regime corresponding to the parameters $Re = 1100$, $H_0/c = 1$, $f = 0.14$, $x_p/c = 1/3$ and $\theta_0 = 76.33^o$ has been computed, see figure 1 for a motion sketch. Autovalidation tests using different mesh sizes and different domain sizes were performed to verify independency of the force predictions, see figure 2. Simulations using two different domains, one domain referenced as Dom1=$[-3:8]\times[-4:4]$ and the other one referenced as Dom2=$[-3:8]\times[-8:8]$, have been performed to investigate boundary conditions effects on the solution. Figure 2(a) demonstrates a very good agreement between the two solutions and then Dom1 is sufficient to obtain a correct solution. Figures 2(b), (c) and (d) compare C_x, C_y and C_m obtained with three different meshes corresponding to $dx = 5\times 10{-}3$, $dx = 2\times 10^{-3}$ and $dx = 1\times 10^{-3}$ and show a grid convergence of the method. Following those tests the further solutions presented are obtained using the smaller domain, Dom1=$[-3:8]\times[-4:4]$, and a mesh spacing of $dx = 2\times 10^{-3}$. To validate our numerical results we check our forces predictions against the results presented by Kinsey et al. [8]. Results of instantaneous forces, C_x, C_y and pitching moments C_m, figure 3, for the high-efficiency power extraction case are in good agreements with Kinsey's results.

The operating regime of an airfoil oscillating at a given frequency can be change by varying the pitching amplitude θ_0. Therefore, a propulsion regime corresponding to the parameters $Re = 1100$, $H_0/c = 1$, $f = 0.14$, $x_p/c = 1/3$ and $\theta_0 = 20^o$ has also been

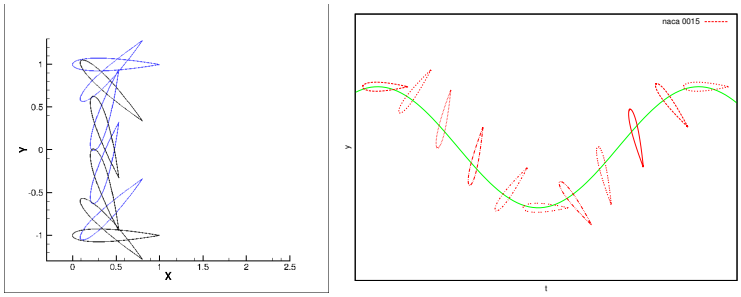

Figure 1: Sketch of the airfoil motion, power-extraction regime, for $H_0/c = 1$, $f = 0.14$, $x_p/c = 1/3$ and $\theta_0 = 76.33^o$.

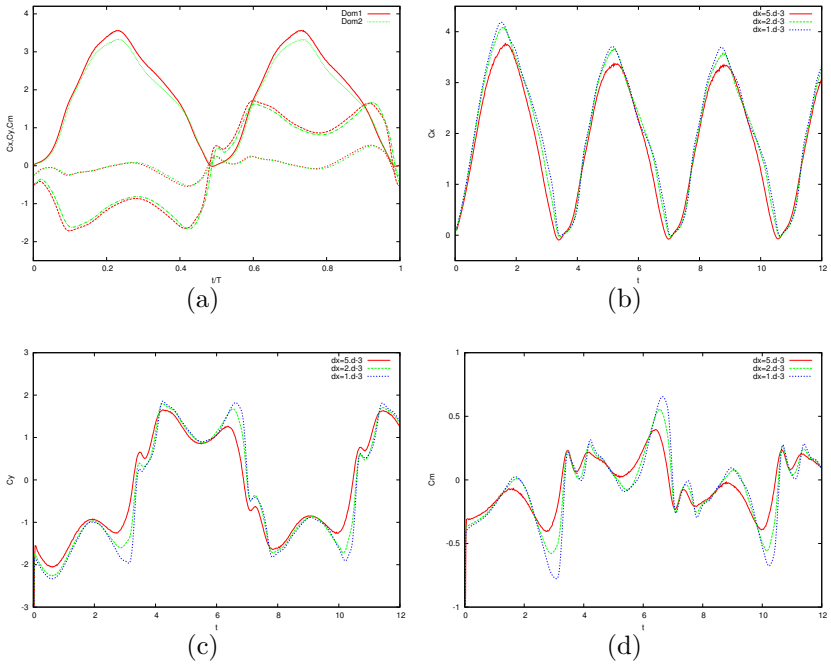

Figure 2: (a) Influence of the domain size on calculated forces and momenyt, Dom1 = $[-3:8]\times[-4:4]$, Dom2=$[-3:8]\times[-8:8]$. Mesh sensitivity on the drag coefficient (b) on the lift coefficient (c) and on the pitching moment (d).

selected. The motion description is sketched in figure 4 and the calculated drag coefficient, lift coefficient and pitching moment are presented in figure 5. Again, the results are in good agreement with the published results of Kinsey et al. [8].

4.2 Study of the airfoil geometry effect

On the power extraction regime, $Re = 1100$, $H_0/c = 1$, $f = 0.14$, $x_p/c = 1/3$ and $\theta_0 = 76.33^o$, we study the effect of different NACA airfoil profiles drawn in figures 6 and 8(a) on the forces and pitching moment. The airfoils on figure 6 (a) and 8(a) are

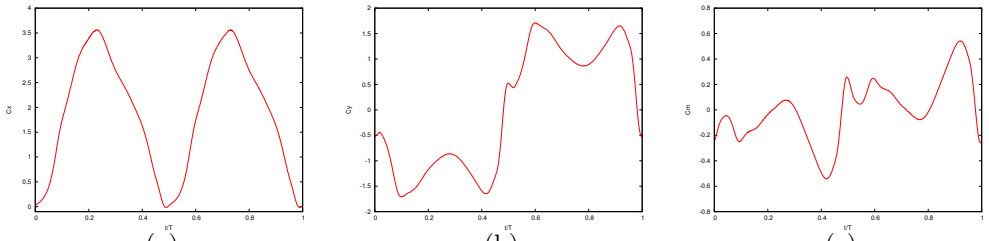

(a) (b) (c)

Figure 3: Power-extraction results on a NACA 0015 airfoil (a) Drag coefficient, (b) Lift coefficient, (c) Pitching moment.

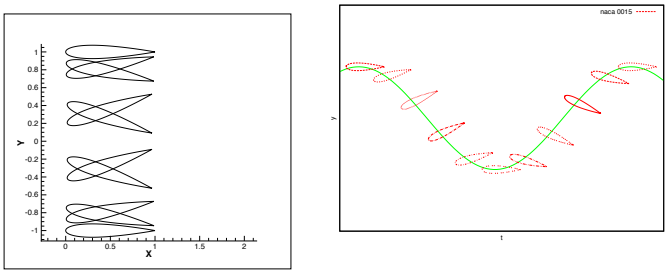

Figure 4: Propulsion, for $H_0/c = 1$, $f = 0.14$, $x_p/c = 1/3$ and $\theta_0 = 20.^o$.

symmetric, the ones on 6 (b) are cambered.

On figure 7, the forces and pitching moments are compared for four and five digit NACA geometries. All the curves are similar in shape, however the maximum values sligthly decrease as the airfoil thickness increases. The six digit airfoil of figure 8(a) is a laminar airfoil with a design lift coefficient of 0 and should maintain a laminar flow all over the airfoil. The results are still similar, with higher maximum values when compare to the reference NACA 0015 airfoil, probably caused by the difference in thickness values.

5 CONCLUSIONS

An IBM based on penalization and VIC methods has been used to study the aerodynamic forces acting on an airfoil in flapping motion. The aerodynamic forces and moment are computed from the penalization term added to the momentum equation. Predicted force and moment agree with literature. The flapping motion has been imposed to several airfoil shapes. At this low Reynolds number, geometry effects are small. Generally, increasing the airfoil thickness decreases the maximum values for the forces and moment.

REFERENCES

[1] R. Mittal, and G. Iaccarino, Immersed Boundary Methods. *Annu. Rev. Fluid. Mech.*, Vol. **37**, p. 239-261, 2005.

[2] J. T. Rasmussen, G. H. Cottet, J. H. Walther, A multiresolution remeshed Vortex-In-Cell algorithm using patches. *Journal of Computational Physics*, Vol. **230**, p. 6742–6755, 2011

[3] F. Capizzano, Turbulent Wall Model for Immersed Boundary Methods. *AIAA Journal*, Vol. **49**, No. 11, 2011

[4] R. Ghias, R. Mittal, and H. Dong, A Sharp Interface Immersed Boundary Method for Compressible Viscous Flows. *Journal of Computational Physics*, Vol. **225**, p. 528-553, 2007

[5] B. Kadoch, D. Kolomenskiy, P. Angot, K. Schneider, A Volume Penalization Method for Incompressible Flows and Scalar Advection-diffusion with Moving Obstacle. *Journal of Computational Physics*, Vol. **231**, p. 4365-4383, 2012.

[6] R. E. Harris, Adaptive Cartesian Immersed Boundary Method for Simulation of Flow over Flexible Geometries. *AIAA Journal*, Vol. **51**, No. **1**, 2013, p. 53–69

[7] X. Q. Zhang, P. Theissen, and J. U. Schlüter, Towards simulation of flapping wings using immersed boundary method. *International Journal for Numerical Methods in Fluids*, Vol. **71**, p. 522-536

[8] T. Kinsey and G. Dumas. Parametric Study of an Oscillating Airfoil n a Power-Extraction Regime. *AIAA Journal*, Vol. **46**, No. **6**, p. 543–561, 2008.

[9] F. Morency, H. Beaugendre, F. Gallizio, Aerodynamic force evaluation for ice shedding phenomenon using vortex in cell scheme, penalisation and level set approaches. *International Journal of Computational Fluid Dynamics*, Vol. **26**, No. **9-10**, p. 435–450, 2012.

[10] Coquerelle, M. and Cottet, G. H., A vortex level set method for the two-way coupling of an incompressible fluid with colliding rigid bodies,, *JCP*, Vol. **227**, No. **21**, p. 9121–9137, 2008.

[11] Cottet, G. H. and Michaux, B. and Ossia, S. and VanderLinden, G., A comparison of spectral and vortex methods in three-dimensional incompressible flows, *JCP*, Vol. **175**, No. **2**, p. 702–712, 2002.

[12] Monaghan, J. J., Extrapolating B splines for interpolation, *JCP*, Vol. **60**, No. **2**, p. 253–262, 1985.

[13] F. Noca, D. Shiels, and D. Jeon, A comparison of methods for evaluating time-dependent fluid dynamic forces on bodies, using only velocity fields and their derivatives. *Journal of Fluids and Structures*. Vol. **13**,p. 571–578, 1999.

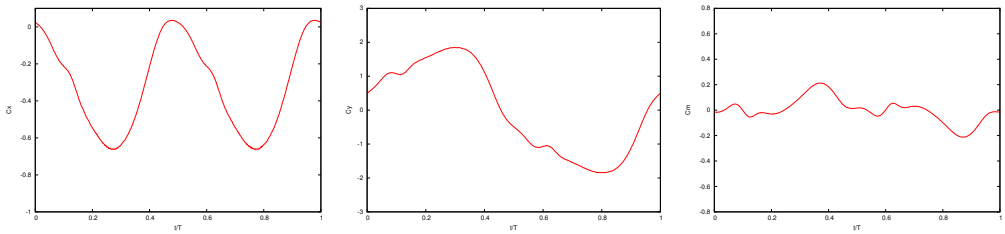

(a) (b) (c)

Figure 5: Propulsion results on a NACA 0015 airfoil (a) Drag coefficient, (b) Lift coefficient, (c) Pitching moment.

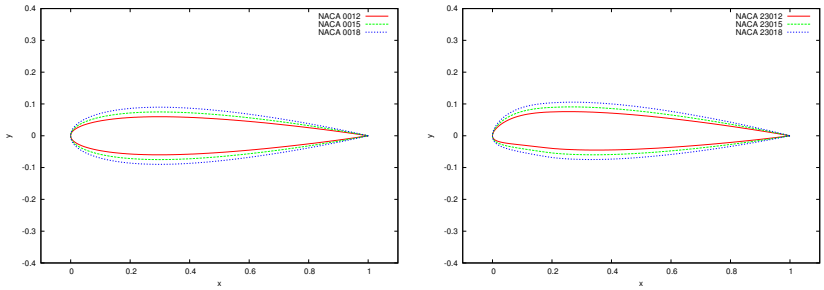

(a) (b)

Figure 6: NACA airfoil profiles.

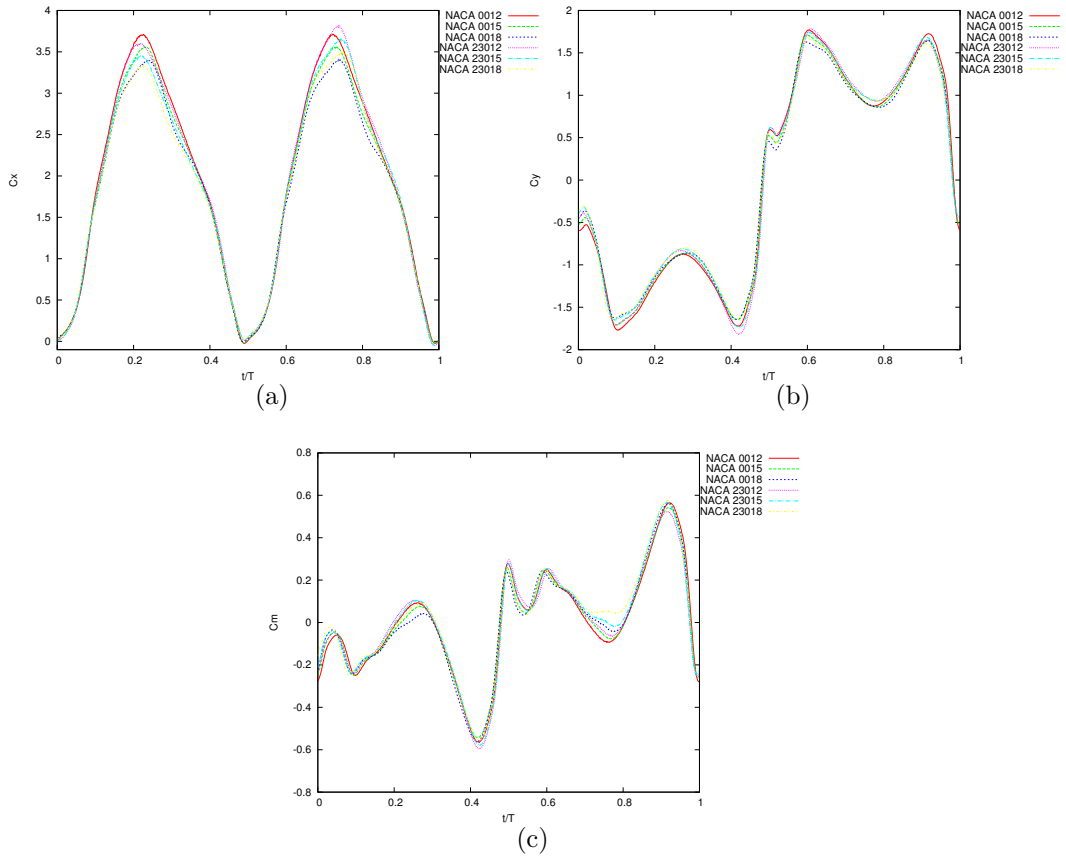

Figure 7: Comparison of forces and pitching moment for different NACA geometries, left: drag coefficient, middle: lift coefficient, right: pitching moment coefficient.

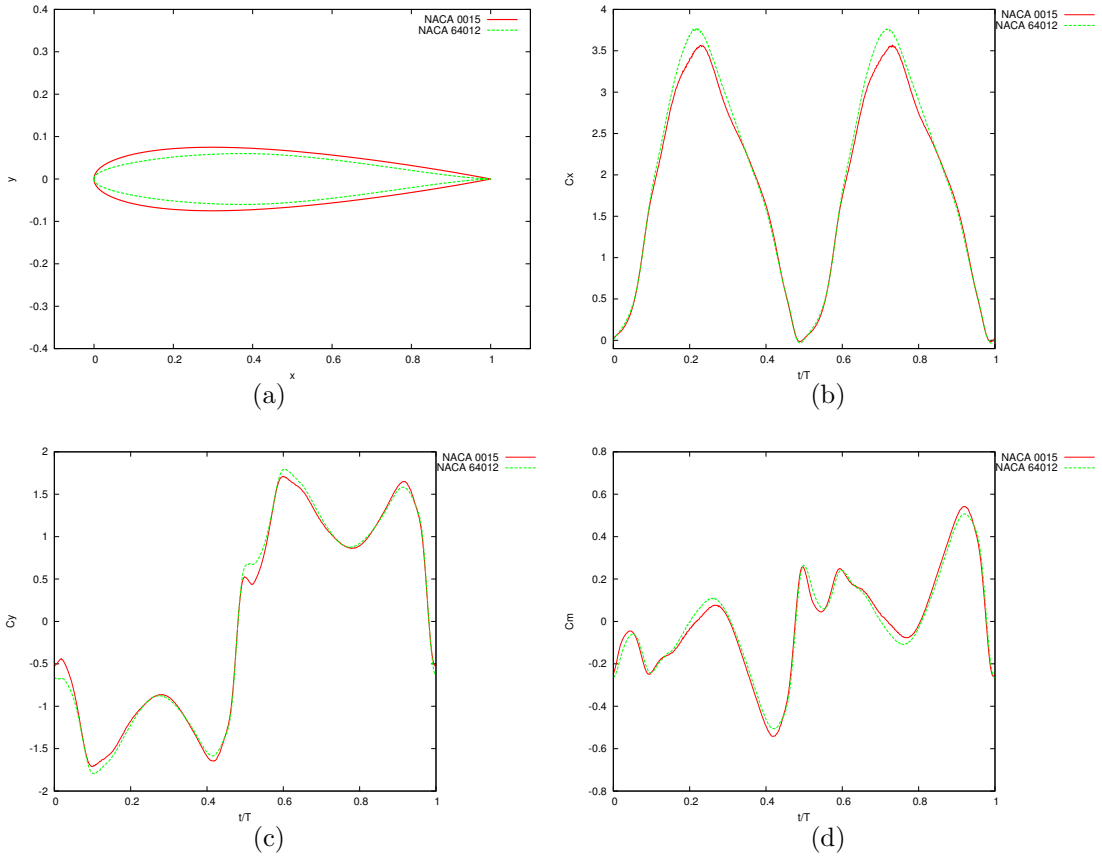

Figure 8: Comparison between a NACA 0015 airfoil and a NACA $64_1 - 012$ a=1.0 airfoil.